1   # Plagioclase archives of depleted melts in the oceanic crust

2   **David A. Neave[1,2] and Olivier Namur[3]**

3   *[1]Department of Earth and Environmental Sciences, The University of Manchester, M13 9PL*

4   *Manchester, UK*

5   *[2]Leibniz Universität Hannover, Institut für Mineralogie, 30167 Hannover, Germany*

6   *[3]Department of Earth and Environmental Sciences, KU Leuven, BE-3001 Leuven, Belgium*

7   **ABSTRACT**

8   Mid-ocean ridge and ocean island basalts provide vital but incomplete insights into mantle

9   chemistry. For example, high-anorthite plagioclase is generally too refractory and incompatible-

10   element depleted to have crystallized from the melts that carry it to the surface. Moreover,

11   erupted basalts rarely preserve the extreme isotopic and incompatible-element depletions found

12   in some primitive melt inclusions and residual abyssal peridotites. By integrating experimental

13   observations with analyses of natural crystals and glasses, we infer that high-anorthite

14   plagioclase grows from high-degree melts of refractory but otherwise unexotic mantle sources

15   with depleted incompatible element compositions. The widespread occurrence of high-anorthite

16   plagioclase in oceanic basalts and the oceanic crust hence indicates that refractory melts pervade

17   the uppermost mantle and lower crust. We thus suggest that refractory melts play much a greater

18   role in crustal accretion than typically recognized, and that refractory and feasibly depleted

19   peridotite is more prevalent in the upper mantle than previously thought.

20   **INTRODUCTION**

21   Mid-ocean-ridge and ocean-island basalts (MORB and OIB respectively; oceanic basalts

22   collectively) provide important windows into the chemistry of Earth's mantle (Hofmann, 1997;

23   Stracke, 2021). Over billions of years, lithospheric recycling at subduction zones has created

24   chemically, isotopically and lithologically enriched mantle domains that are ultimately reflected

25   in the compositions of erupted basalts (Chase, 1981). Concurrent melt extraction and crustal

26   accretion has created refractory and depleted domains that are well documented in abyssal

27   peridotites but rarely expressed in erupted records, reflecting the poor preservation of depleted

28   melts (Salters et al., 2011; Byerly and Lassiter, 2014; Sanfilippo et al., 2021). Melt inclusions in

29   primitive crystals, which are relatively resistant to mixing-induced overprinting, thus provide vital

30   constraints on the chemical and isotopic variability of primitive melts and their mantle sources

31   (Sobolev and Shimizu, 1993; Maclennan, 2008b, 2008a; Stracke et al., 2019). They are however

32   challenging to analyze and remain susceptible to contamination by enriched melts in the deepest

33   reaches of plumbing systems. Fortunately, crystals also record information about the melts from

34   which they grow, and as volumetrically significant components of magmas and cumulates can

35   reflect the abundance of chemically distinct melts at depth.

36   High-anorthite plagioclase ($X_{An} > 0.8$, where $X_{An} =$ molar Ca/(Ca+Na+K)) is a major

37   constituent of many basalts from ocean islands and slow- to intermediate-spreading mid-ocean

38   ridges (Lange et al., 2013), as well as various cumulates from ophiolites and the lower oceanic

39   crust (Browning, 1982; Lissenberg et al., 2013). However, such crystals are rarely in major-

40   element equilibrium with erupted basalts (cf. Natland et al., 1983). Moreover, they are often out

41   of isotopic and incompatible-element equilibrium with their carrier melts, implying origins from

42   different mantle melt distributions (Halldórsson et al., 2008; Neave et al., 2014; Nielsen et al.,

43   2020). High-X_{An} plagioclase cannot be reproduced in experiments on MORB starting

44   compositions with realistic volatile contents (Grove et al., 1992; Kohut and Nielsen, 2003), and

45   calculations with the MELTS algorithm indicate that primitive MORBs (MgO > 8 wt.%)

46   typically saturate in X_{An} = 0.75–0.80 plagioclase (Ghiorso and Sack, 1995; Neave et al., 2019).

47   High-X_{An} plagioclase crystals in oceanic settings are hence thought to grow from refractory,

48   high-Ca# melts (where Ca# = molar Ca/(Ca+Na)) with high solidus and liquidus temperatures

49   that seldom erupt (Grove et al., 1992; Neave et al., 2019). Here we integrate observations from

50   natural and experimental systems to explore the origins of high-X_{An} plagioclase crystals in

51   oceanic settings and discuss the role that high-Ca# melts play in oceanic magmatism.

52   **PLAGIOCLASE-LIQUID EQUILIBRIA**

53   The exchange of anorthite (An; $CaAl_2Si_2O_8$) and albite (Ab; $NaAlSi_3O_8$) components

54   between liquid and plagioclase depends on many variables (Namur et al., 2012, and references

55   therein). In summary, equilibrium plagioclase X_{An} correlates positively with melt Ca#, melt Al#

56   (where Al# = molar Al/(Al+Si)), melt H_2O content and temperature, and negatively with

57   pressure. The melt H_2O content of oceanic basalts is uniformly low when compared with arc

58   basalts (≤1 wt.%; Michael, 1995), and thus exerts little influence over plagioclase X_{An}.

59   Conversely, melt Ca#, which varies greatly in oceanic basalts, is inextricably linked with

60   equilibrium X_{An} and the timing of plagioclase saturation (Bowen, 1913). For example,

61   observations from experiments on synthetic analogues of Icelandic lavas at 300 MPa

62   demonstrate that plagioclase saturates at higher melt MgO contents and temperatures, and with

63   higher X_{An} contents, during the crystallization of high-Ca# primitive melts from depleted

64   peridotite sources with refractory major element compositions than during the crystallization of

65   low-Ca# primitive melts from modally enriched sources with more fusible compositions (Neave

66   et al., 2019). To place these observations within the polybaric context of crustal magmatism, we

67   performed new crystallization experiments on the same lava analogues from Iceland at 100 and

68   600 MPa (high-Ca# Háleyjabunga lava, refractory source; low-Ca# Stapafell lava, fusible

69   source; details in the Supplementary Material).

70   Plagioclase-liquid equilibria at 100 and 600 MPa are summarized in Fig. 1 alongside

71   published equilibria at 300 MPa from Neave et al. (2019). The high-Ca# Háleyjabunga analogue

72   saturates in plagioclase at higher melt MgO contents (and temperatures) than the low-Ca#

73   Stapafell analogue. While isobaric differences in plagioclase saturation between the two starting

74   compositions reflect mantle-derived variability in melt Ca# and Al#, polybaric differences reflect

75   differences in plagioclase and clinopyroxene stability, with plagioclase generally saturating at

76   lower temperatures (and melt MgO contents) when clinopyroxene stability is greater at higher

77   pressures (Fig. 1). Equilibrium plagioclase X_{An} also correlates negatively with clinopyroxene

78   stability and pressure. Overall, melt composition, which correlates with pressure and temperature

79   as well as source composition, exerts the main control over X_{An}, with high-X_{An} plagioclase only

80   crystallizing from the high-Ca# Háleyjabunga analogue (up to $X_{An} = 0.88$ and 0.85 in the

81   products of 100 and 300 MPa experiments, respectively; the highest X_{An} crystallized from low-

82   Ca# Stapafell analogue was 0.71). Importantly, our new experiments demonstrate that high-X_{An}

83   plagioclase can be produced from refractory oceanic basalts under realistic pressure and

84   temperature conditions (cf. Grove et al., 1992; Kohut and Nielsen, 2003). Even if the

85   composition of Háleyjabunga lava is at the limit of erupted variability (Fig. 3), our findings thus

86   suggest high-X_{An} plagioclase crystals reflect the crystallization of refractory but essentially

87   unexotic melts derived from refractory mantle sources that experienced high degrees of prior

88   melt extraction, whether recent or ancient.

89   **PREDICTING PLAGIOCLASE-LIQUID EQUILIBRIA**

90   By predicting equilibrium plagioclase X_{An} as a function of melt composition it is possible

91   to evaluate plagioclase-liquid equilibria in diverse natural systems. While thermodynamic

92   models allow phase relations to be extrapolated across wide parameter spaces (Ghiorso and Sack,

93   1995; Holland et al., 2018), empirical models can be more precise when applied within their

94   calibration ranges (e.g., Namur et al., 2012). Moreover, it is possible to avoid introducing

95   erroneous assumptions about crystallization conditions by predicting equilibrium X_{An} from melt

96   compositions alone; pressure and temperature are implicit in melt compositions.

97   Performing multiple linear regression through calibration data ($n = 98$) from experimental

98   studies on basalts from mid-ocean ridges, an oceanic plateau and an ocean island yields the

99   following relationship between plagioclase X_{An} and melt composition (Fig. 2a; $r^2 = 0.88$;

100   standard error = 0.03; details and sources in the Supplementary Material):

101         $X_{An} = 0.92(0.07) \cdot Ca\#_{melt} + 1.63(0.24) \cdot Al\#_{melt} + 0.24(0.05) \cdot (molar\ Ca/Al)_{melt} - 0.54(0.06)$ (1)

102   Test data ($n = 36$) from experimental studies on basalts from mid-ocean ridges and a continental

103   hotspot with $X_{An} \sim 0.6$–0.9 are reproduced well by equation 1 ($r^2 = 0.92$; standard error = 0.02),

104   albeit with a slight offset to lower X_{An}, possibly because of Na loss during some experiments

105   (Fig. 2b; sources in the Supplementary Material).

106   **ORIGINS OF HIGH-ANORTHITE PLAGIOCLASE**

107   High-X_{An} plagioclase has been described in lavas from many mid-ocean ridge segments

108   and ocean islands (e.g., Lange et al., 2013). Here we apply our model to published Icelandic and

109   MORB glass compositions, though our findings are likely to apply in other settings erupting

110   H_2O-poor basalts. Equilibrium plagioclase X_{An} predicted from Icelandic ($n = 190$) and MORB (n

111     $= 1687$) glass compositions collated by Shorttle and Maclennan (2011) and Gale et al. (2013),

112   respectively, are shown in Fig. 3; results were filtered for plagioclase saturation using a stability

113   criterion from Gale et al. (2014) (details in the Supplementary Material).

114   Predicted plagioclase X_{An} correlates with melt MgO content and Ca# in Icelandic and

115   MORB datasets (Figs. 3A and 3B), though high-Ca# melts occur across a wide range of melt

116   MgO contents (8–11 wt.%). Crucially, some glasses from both datasets return stable high-X_{An}

117   compositions ($n = 33$ and 22, respectively). Although these glasses are at the limit of natural

118   variability in the case of MORB, their occurrence nonetheless substantiates rare observations of

119   equilibrium high-X_{An} in nature (X_{An} up to 0.89; Natland et al., 1983). Icelandic glasses return

120   higher maximum X_{An} contents than MORB glasses (up to $X_{An} = 0.89$ and 0.85, respectively),

121   likely reflecting differences in sampling density and mantle melting conditions.

122   As well as being associated with high melt Ca# at any given melt MgO content (Figs. 3A

123   and 3B), high-X_{An} plagioclase is typically associated with low melt K_2O contents (often

124   <0.1 wt.%; Figs. 3C and 3D), recapitulating the incompatible-element-depleted character of

125   erupted high-X_{An} plagioclase (Neave et al., 2014; Nielsen et al., 2020). Such high-Ca#, low-K_2O

126   melts are commonly generated by shallow melting of refractory peridotites that have experienced

127   high degrees of prior melting (e.g., Grove et al., 1992; Shorttle and Maclennan, 2011). High-X_{An}

128   plagioclase is also associated with low melt FeO* contents (total Fe as FeO) at any given melt

129   MgO content (Figs 3E and 3F). This is particularly clear for Iceland, where low-FeO* primitive

130   melts (FeO* < 10 wt.%) from relatively refractory peridotites are predicted to be equilibrium in

131   with high-X_{An} plagioclase but high-FeO* primitive melts (FeO* > 10 wt.%) from modally

132   enriched sources (pyroxenites *sensu lato*) are not predicted to be in equilibrium with plagioclase

133   of any composition (Fig. 3E). Refractory melts capable of crystallizing high-X_{An} plagioclase thus

134   do not mix substantially with melts from modally enriched sources during ascent and are derived

135   from dominantly peridotitic sources (Shorttle and Maclennan, 2011); rare K_2O-rich melts in

136   equilibrium with high-X_{An} plagioclase may have interacted with depleted harzburgites (Fig. 3D;

137   Nielsen et al., 2020). We hence argue that high-X_{An} plagioclase crystals are the solid products of

138   melts from sources that have experienced high degrees of prior melting. In some cases, isotopic

139   depletions suggest that this melt extraction was ancient (Halldórsson et al., 2008; Nielsen et al.,

140   2020). Indeed, we speculate that high-X_{An} plagioclase may be associated with ultra-depleted

141   sources recorded by some melt inclusions and abyssal peridotites (Sobolev and Shimizu, 1993;

142   Salters et al., 2011; Stracke et al., 2019), though closer integration of isotopic and major-element

143   observations is required to test this further.

WIDESPREAD REFRACTORY MELTS AT DEPTH

145   High-X_{An} plagioclase occurs throughout the oceanic realm (Fig. 4). In Iceland, it is

146   especially well documented in the Eastern Volcanic Zone (Fig. 4A), where isotopically and

147   incompatible-element-depleted high-X_{An} plagioclase may constitute >30 vol.% of lavas with

148   comparatively enriched isotopic and incompatible-element compositions (Halldórsson et al.,

149   2008). High-X_{An} plagioclase has also been described in depleted picrites from Iceland's Northern

150   Volcanic Zone of Iceland, as well as in diverse basalts from Galápagos, Réunion and Kerguelen

151   (Fig. 4A). Overall, these observations suggest that refractory melts with depleted incompatible-

152   element compositions are more prevalent beneath ocean islands than the incompatible-element

153   enriched character of OIBs would otherwise imply (e.g., Stracke et al., 2019).

154   High-X_{An} plagioclase crystals have been widely reported in plagioclase-rich MORBs

155   from slow- to intermediate-spreading mid-ocean ridges (Fig. 4B; Lange et al., 2013; Nielsen et

156   al., 2020). With a few notable exceptions (Fig. 4B; Natland et al., 1983), these high-X_{An} contents

157   are found in crystal cores surrounded by more evolved rims and are out of equilibrium with their

158 carrier melts, mirroring observations from ocean islands that high-Ca# melts from refractory

159 sources are probably more widespread at depth than suggested by erupted archives. Indeed, melt

160 inclusion entrapment pressures typically place high-X_{An} plagioclase crystallization at or below

161 the Moho (Drignon et al., 2018), preventing the eruption of such plagioclase in many settings.

162 Recent experiments have also suggested that phase relations at >500 MPa may play a key role in

163 generating X_{An} ~ 0.9 plagioclase (Ustunisik et al., 2022).

164   High-X_{An} plagioclase crystals are found in lower crustal sections of the fast-spreading

165 Samail ophiolite in Oman (Fig. 4C; Browning, 1982), though elevated melt H_2O contents likely

166 modify plagioclase-liquid equilibria in ophiolitic settings (Koepke et al., 2021). Despite its

167 relative scarcity, perhaps as a result of melt rock-reaction (Sanfilippo et al., 2020), X_{An} ~ 0.8

168 plagioclase does occur in crustal samples from the fast-spreading East Pacific Rise, slow-

169 spreading Mid-Atlantic Ridge and very slow-spreading Southwest Indian Ridge (Fig. 4D; Dick

170 et al., 2002; Lissenberg et al., 2013; Sanfilippo et al., 2019), suggesting that high-Ca# melts

171 occur and contribute to crustal accretion throughout the global ridge system. Observations from

172 the East Pacific Rise also illustrate how magmatic processes bias records of chemical variability,

173 with high-X_{An} present at depth but absent from seafloor lavas as a consequence of filtering by

174 axial melt lenses.

175   In line with observations from melt incluions and abyssal peridotites, we argue that the

176 global occurrence of high-X_{An} plagioclase demonstrates that refractory and incompatible

177 element-depleted melts occur widely in the uppermost mantle and lower crust. Two key

178 implications of this are that melts from refractory mantle sources are likely to play a greater role

179 in crustal accretion than currently recognized and that refractory (and feasibly depleted) domains

180 may be more prevalent in the upper mantle than previously thought.

181

186 **REFERENCES CITED**

187 Bowen, N.L., 1913, The melting phenomena of the plagioclase feldspars: American Journal of

188   Science, v. 35, p. 577–599, doi:10.2475/ajs.s4-35.210.577.

189 Browning, P., 1982, The petrology, geochemistry and structure of the plutonic rocks of the

190   Oman ophiolite: Open University, 404 p., doi:10.21954/ou.ro.0000de14.

191 Byerly, B.L., and Lassiter, J.C., 2014, Isotopically ultradepleted domains in the convecting upper

192   mantle: Implications for MORB petrogenesis: Geology, v. 42, p. 203–206,

193   doi:10.1130/G34757.1.

194 Chase, C.G., 1981, Oceanic island Pb: Two-stage histories and mantle evolution: Earth and

195   Planetary Science Letters, v. 52, p. 277–284, doi:10.1016/0012-821X(81)90182-5.

196 Danyushevsky, L. V., 2001, The effect of small amounts of H_2O on crystallisation of mid-ocean

197   ridge and backarc basin magmas: Journal of Volcanology and Geothermal Research, v. 110,

198   p. 265–280, doi:10.1016/S0377-0273(01)00213-X.

199 Dick, H.J.B. et al., 2002, Primary silicate mineral chemistry of a 1.5-km section of very slow

200   spreading lower ocean crust: ODP Hole 735B, Southwest Indian Ridge: Proceedings of the

201   Ocean Drilling Program, Scientific Results, v. 176, doi:10.2973/odp.proc.sr.176.001.2002.

202   Drignon, M.J., Nielsen, R.L., Tepley, F.J., and Bodnar, R.J., 2018, Upper mantle origin of

203   plagioclase megacrysts from plagioclase-ultraphyric mid-oceanic ridge basalt: Geology, v.

204   47, p. 1–4, doi:10.1130/G45542.1.

205   Gale, A., Dalton, C.A., Langmuir, C.H., Su, Y., and Schilling, J.G., 2013, The mean composition

206   of ocean ridge basalts: Geochemistry, Geophysics, Geosystems, v. 14, p. 489–518,

207   doi:10.1029/2012GC004334.

208   Gale, A., Langmuir, C.H., and Dalton, C.A., 2014, The Global Systematics of Ocean Ridge

209   Basalts and their Origin: Journal of Petrology, v. 55, p. 1051–1082,

210   doi:10.1093/petrology/egu017.

211   Ghiorso, M.S., and Sack, R.O., 1995, Chemical mass transfer in magmatic processes IV. A

212   revised and internally consistent thermodynamic model for the interpolation and

213   extrapolation of liquid-solid equilibria in magmatic systems at elevated temperatures and

214   pressures: Contributions to Mineralogy and Petrology, v. 119, p. 197–212,

215   doi:10.1007/BF00307281.

216   Grove, T.L., Kinzler, R.J., and Bryan, W.B., 1992, Fractionation of Mid-Ocean Ridge Basalt

217   (MORB), *in* Mantle Flow and Melt Generation at Mid-Ocean Ridges, Geophysical

218   Monograph 71, Washington D.C., American Geophysical Union, p. 281–310,

219   doi:0.1029/GM071.

220   Halldórsson, S.A., Óskarsson, N., Grönvold, K., Sigurdsson, G., Sverrisdottir, G., and

221   Steinthórsson, S., 2008, Isotopic-heterogeneity of the Thjorsa lava-Implications for mantle

222   sources and crustal processes within the Eastern Rift Zone, Iceland: Chemical Geology, v.

223   255, p. 305–316, doi:10.1016/j.chemgeo.2008.06.050.

224   Hofmann, A.W., 1997, Mantle geochemistry: the message from oceanic volcanism: Nature, v.

225   385, p. 219–229, doi:10.1038/385219a0.

226   Holland, T.J.B., Green, E.C.R., and Powell, R., 2018, Melting of peridotites through to granites:

227   a simple thermodynamic model in the system KNCFMASHTOCr: Journal of Petrology, v.

228   59, p. 881–900, doi:10.1093/petrology/egy048.

229   Koepke, J., Feig, S.T., Berndt, J., and Neave, D.A., 2021, Wet magmatic processes during the

230   accretion of the deep crust of the Oman Ophiolite paleoridge: Phase diagrams and

231   petrological records: Tectonophysics, v. 8, p. 229051, doi:10.1016/j.tecto.2021.229051.

232   Kohut, E.J., and Nielsen, R.L., 2003, Low-pressure phase equilibria of anhydrous anorthite-

233   bearing mafic magmas: Geochemistry, Geophysics, Geosystems, v. 4, p. 1–27,

234   doi:10.1029/2002GC000451.

235   Lange, A.E., Nielsen, R.L., Tepley, F.J., and Kent, A.J.R., 2013, The petrogenesis of

236   plagioclase-phyric basalts at mid-ocean ridges: Geochemistry, Geophysics, Geosystems, v.

237   14, p. 3282–3296, doi:10.1002/ggge.20207.

238   Lissenberg, C.J., MacLeod, C.J., Howard, K.A., and Godard, M., 2013, Pervasive reactive melt

239   migration through fast-spreading lower oceanic crust (Hess Deep, equatorial Pacific

240   Ocean): Earth and Planetary Science Letters, v. 361, p. 436–447,

241   doi:10.1016/j.epsl.2012.11.012.

242   Maclennan, J., 2008a, Concurrent mixing and cooling of melts under Iceland: Journal of

243   Petrology, v. 49, p. 1931–1953, doi:10.1093/petrology/egn052.

244 Maclennan, J., 2008b, Lead isotope variability in olivine-hosted melt inclusions from Iceland:

245   Geochimica et Cosmochimica Acta, v. 72, p. 4159–4176, doi:10.1016/j.gca.2008.05.034.

246 Michael, P.J., 1995, Evidence from trace elements and H_2O for regionally distinctive sources of

247   depleted MORB: Implications for evolution of the depleted mantle: Earth and Planetary

248   Science Letters, v. 131, p. 301–320, doi:10.1180/minmag.1994.58A.2.52.

249 Namur, O., Charlier, B., Toplis, M.J., and Vander Auwera, J., 2012, Prediction of plagioclase-

250   melt equilibria in anhydrous silicate melts at 1-atm: Contributions to Mineralogy and

251   Petrology, v. 163, p. 133–150, doi:10.1007/s00410-011-0662-z.

252 Natland, J.H., Adamson, A.C., Laverne, C., Melson, W.G., and O'Hearn, T., 1983, A

253   Compositionally Nearly Steady-State Magma Chamber at the Costa Rica Rift: Evidence

254   from Basalt Glass and Mineral Data, Deep Sea Drilling Project Sites 501, 504, and 505, *in*

255   Initial Reports of the Deep Sea Drilling Project, 69, v. 53, p. 1689–1699,

256   doi:10.2973/dsdp.proc.69.154.1983.

257 Neave, D.A., Maclennan, J., Hartley, M.E., Edmonds, M., and Thordarson, T., 2014, Crystal

258   storage and transfer in basaltic systems: the Skuggafjöll eruption, Iceland: Journal of

259   Petrology, v. 55, p. 2311–2346, doi:10.1093/petrology/egu058.

260 Neave, D.A., Namur, O., Shorttle, O., and Holtz, F., 2019, Magmatic evolution biases basaltic

261   records of mantle chemistry towards melts from recycled sources: Earth and Planetary

262   Science Letters, v. 520, p. 199–211, doi:10.1016/j.epsl.2019.06.003.

263   Nielsen, R.L., Ustunisik, G., Lange, A.E., Tepley, F.J., and Kent, A.J.R., 2020, Trace Element

264   and Isotopic Characteristics of Plagioclase Megacrysts in Plagioclase Ultraphyric Basalts

265   (PUB): Geochemistry, Geophysics, Geosystems, v. 21, p. 1–24,

266   doi:10.1029/2019GC008638.

267   Salters, V.J.M., Mallick, S., Hart, S.R., Langmuir, C.E., and Stracke, A., 2011, Domains of

268   depleted mantle: New evidence from hafnium and neodymium isotopes: Geochemistry,

269   Geophysics, Geosystems, v. 12, doi:10.1029/2011GC003617.

270   Sanfilippo, A., Dick, H.J.B., Marschall, H.R., Lissenberg, C.J., and Urann, B., 2019,

271   Emplacement and High-Temperature Evolution of Gabbros of the 16.5°N Oceanic Core

272   Complexes (Mid-Atlantic Ridge): Insights Into the Compositional Variability of the Lower

273   Oceanic Crust: Geochemistry, Geophysics, Geosystems, v. 20, p. 46–66,

274   doi:10.1029/2018GC007512.

275   Sanfilippo, A., MacLeod, C.J., Tribuzio, R., Lissenberg, C.J., and Zanetti, A., 2020, Early-Stage

276   Melt-Rock Reaction in a Cooling Crystal Mush Beneath a Slow-Spreading Mid-Ocean

277   Ridge (IODP Hole U1473A, Atlantis Bank, Southwest Indian Ridge): Frontiers in Earth

278   Science, v. 8, p. 1–21, doi:10.3389/feart.2020.579138.

279   Sanfilippo, A., Salters, V.J.M., Sokolov, S.Y., Peyve, A.A., and Stracke, A., 2021, Ancient

280   refractory asthenosphere revealed by mantle re-melting at the Arctic Mid Atlantic Ridge:

281   Earth and Planetary Science Letters, v. 566, p. 116981, doi:10.1016/j.epsl.2021.116981.

282   Shorttle, O., and Maclennan, J., 2011, Compositional trends of Icelandic basalts: Implications for

283   short-length scale lithological heterogeneity in mantle plumes: Geochemistry, Geophysics,

284   Geosystems, v. 12, p. 1–32, doi:10.1029/2011GC003748.

285   Sobolev, A. V., and Shimizu, N., 1993, Ultra-depleted primary melt included in an olivine from

286   the Mid-Atlantic Ridge: Nature, v. 363, p. 151–154, doi:10.1038/363151a0.

287   Stracke, A., 2021, A process-oriented approach to mantle geochemistry: Chemical Geology, v.

288   184, p. 120350, doi:10.1016/j.chemgeo.2021.120350.

289   Stracke, A., Genske, F., Berndt, J., and Koornneef, J.M., 2019, Ubiquitous ultra-depleted

290   domains in Earth's mantle: Nature Geoscience, v. 12, p. 851–855, doi:10.1038/s41561-019-

291   0446-z.

292   Ustunisik, G.K., Nielsen, R.L., and Walker, D., 2022, The Missing Magmas of MOR: Insights

293   from Phase Equilibrium Experiments on Plagioclase Ultraphyric Basalts: Geochemistry,

294   Geophysics, Geosystems, v. 23, p. e2021GC009943, doi:10.1029/2021gc009943.

295

296
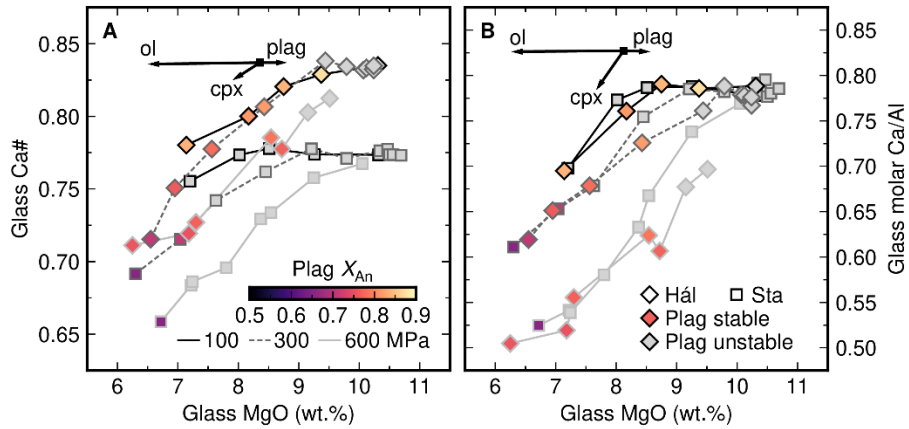
Figure 1. Plagioclase-liquid equilibria in synthetic analogues of the high-Ca# Háleyjabunga (Hál) and low-Ca# Stapafell (Sta) lavas from Iceland (where Ca# = molar Ca/(Ca+Na)) summarized in terms of glass MgO content versus (A) glass Ca# and (B) glass molar Ca/Al. New results at 100 and 600 MPa are presented alongside results at 300 MPa from Neave et al. (2019). Plagioclase crystallizes earlier and with a higher anorthite content (X_{An}, where X_{An} = molar Ca/(Ca+Na+K)) from high-Ca# melts. Vectors show the crystallization of 5 wt.% olivine (ol), clinopyroxene (cpx) and plagioclase (plag) according to Danyushevsky (2001).

304
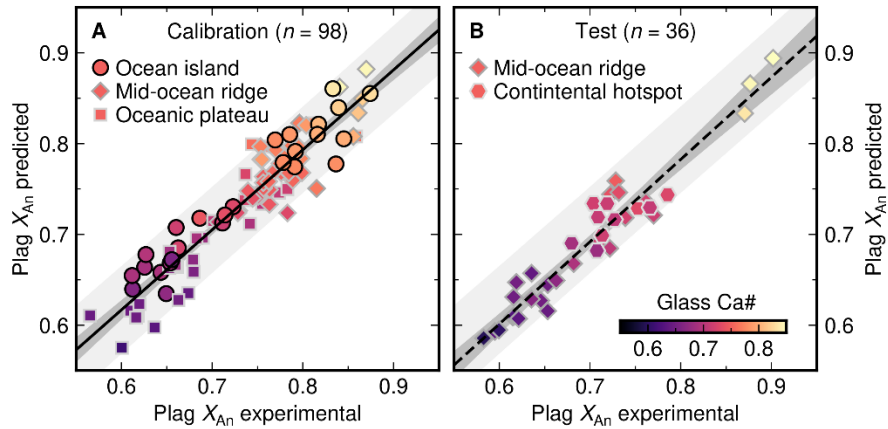
Figure 2. (A) Performance of the multiple linear regression (Eq 1) used to predict plagioclase

(plag) anorthite content (X_{An}) as a function melt composition. The black line shows a regression

through calibration data from experimental studies on basalts from an ocean island, mid-ocean

ridges and an oceanic plateau. Dark and pale grey envelopes show 95% confidence and

prediction intervals, respectively. (B) Performance of Eq 1 on test data from mid-ocean ridges

and a continental hotspot. The dashed black line and dark grey envelope show a regression

through the test data and its 95% confidence interval, respectively; the pale grey envelope shows

the 95% prediction interval of Eq 1. Details and sources in the Supplementary Material.
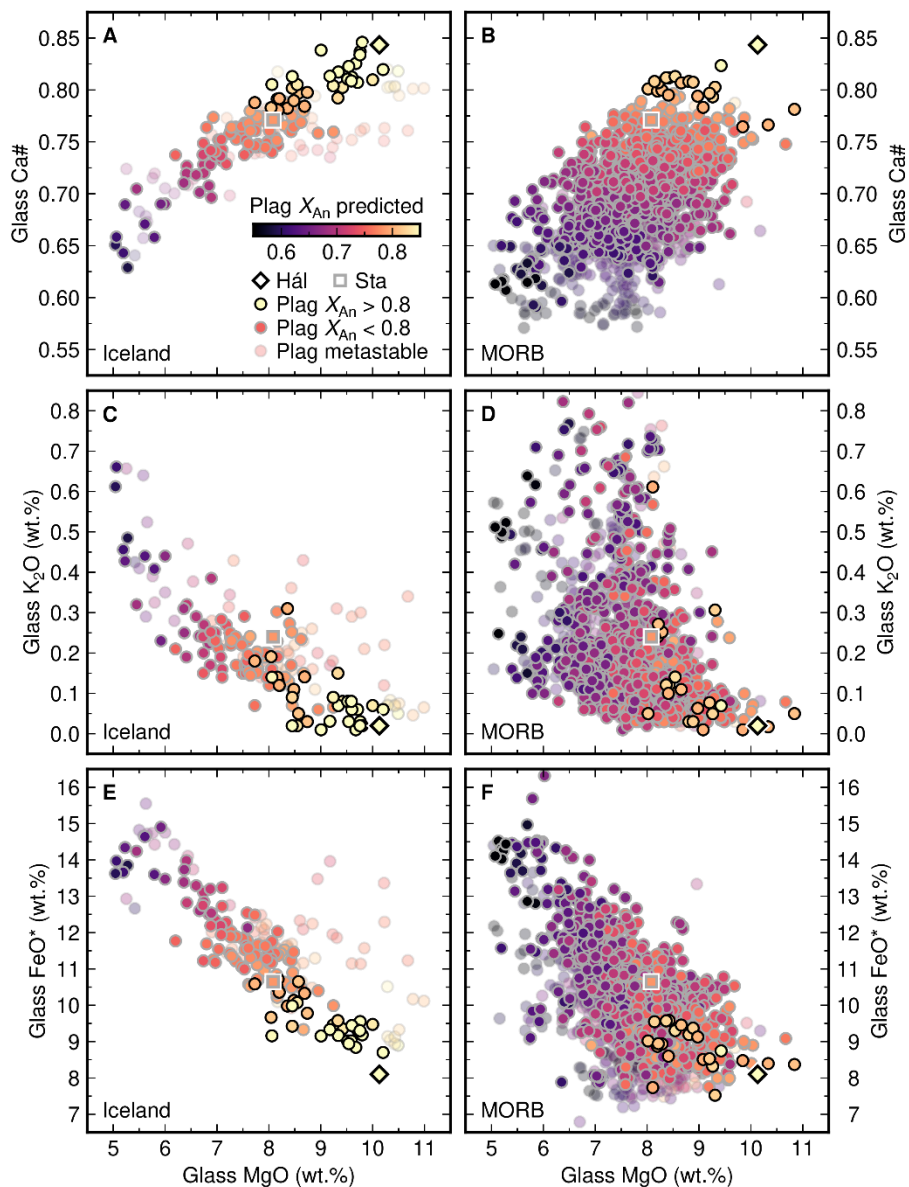
Figure 3. Plagioclase (plag) anorthite contents (X_{An}) predicted to be in equilibrium with Icelandic (A, C and E) and MORB (B, D and F) glasses from Shorttle and Maclennan (2011) and Gale et al. (2013), respectively. The evolution of glass compositions is shown for elements emphasizing fractionation (MgO), degree of source enrichment (K_2O and FeO*) and control on plagioclase-liquid equilibria (Ca#). Glass compositions that fail a plagioclase stability criterion from Gale et al. (2014) are transparent and those in equilibrium with high-X_{An} plagioclase ($X_{An} > 0.8$) are outlined in black; glasses from Háleyjabunga (Hál) and Stapafell (Sta) are highlighted.
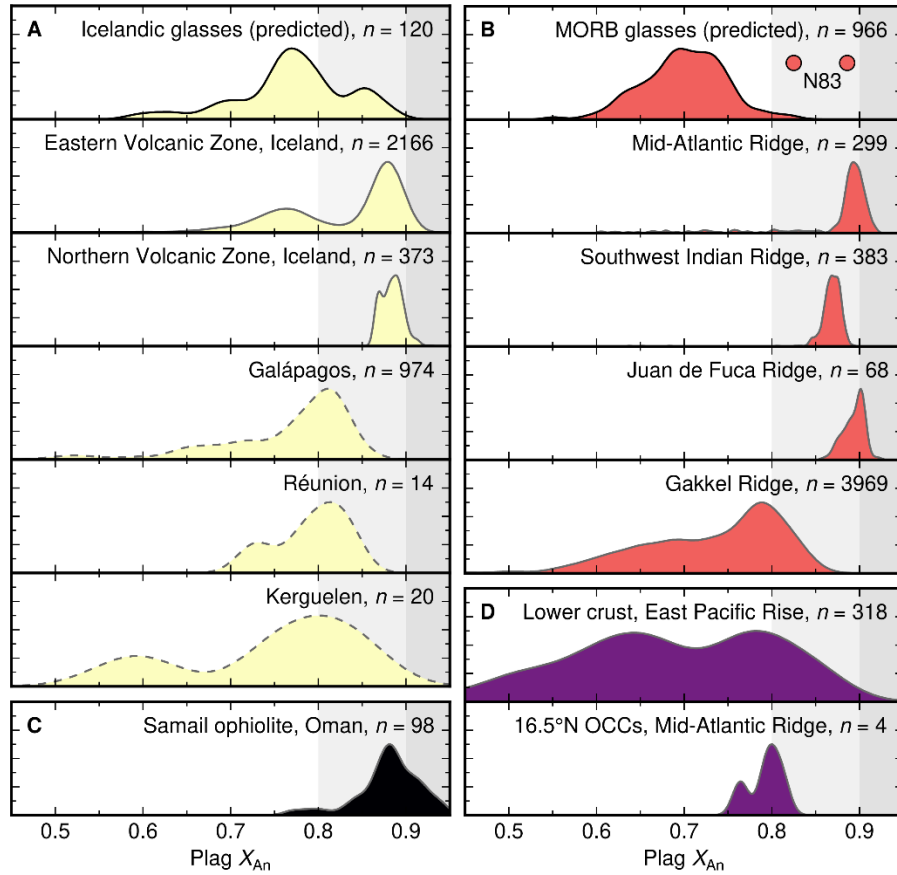
Figure 4. Kernel density estimates summarizing how plagioclase (plag) anorthite contents (X_{An}) predicted to be in equilibrium with (A) Icelandic and (B) MORB glasses from Shorttle and Maclennan (2011) and Gale et al. (2013), respectively, compare with natural plagioclase compositions from (A) ocean island basalts, (B) mid-ocean ridge basalts (MORB), (C) the Samail ophiolite, Oman, and (D) the oceanic crust (OCCs, oceanic core complexes). Rare high-X_{An} rims from MORB are highlighted (Natland et al., 1983; N83). Sources in the Supplementary Material.